Click Here for Full Article

Effects of water table dynamics on regional climate: A case study over east Asian monsoon area

Xing Yuan,[1] Zhenghui Xie,[1] Jing Zheng,[1] Xiangjun Tian,[1] and Zongliang Yang[2]

[1] Groundwater is an important component of the hydrologic cycle, and its anomaly will result in variations of soil moisture, water, and energy balances between the land surface and atmosphere, which ultimately influence climate. In this study, we implement a groundwater model into the regional climate model RegCM3, which is called RegCM3_GW, and investigate the effects of water table dynamics on regional climate. Numerical experiments by RegCM3_GW and RegCM3 over the east Asian monsoon area show that incorporating the water table dynamics into the regional climate model reduces the systematic biases of the simulated precipitation by 38.5% and 39.8% over semiarid and humid regions, respectively, and increases the bias slightly by 5.6% over semihumid regions. To seek the reasons for the differences of simulated precipitation, we analyze the atmospheric water vapor budget and the local water cycle among the water table, soil moisture, evapotranspiration (ET), and convective precipitation. It is found that the top and root zone soil layers become wetter and enhance the bare soil evaporation but do not always increase the transpiration. Because of the variations of each ET's component, the obvious enhancements of ET occur in semiarid regions and contribute to more instable profiles of pseudoequivalent potential temperature. The atmospheric moisture budget analysis indicates that the recycling rate and precipitation efficiency increase greatly over semiarid regions, which presents a local aquifer-atmosphere feedback, while the variations of atmospheric water vapor transport control the development of precipitation over semihumid and humid regions. Therefore, the effects of water table dynamics on regional climate consist of the local aquifer-atmosphere interaction and the changes of circulation originated from ambient aquifer-atmosphere interaction, and the latter factor plays an important role in the monsoon area. Sensitivity of the results to a change in convection parameterization is also explored.

1. Introduction

[2] Groundwater is a crucial source of drinking water throughout the world and the primary source of freshwater besides the glacier. As an essential part of the hydrologic cycle, it is also important in sustaining streams, lakes, wetlands and aquatic communities [*Alley et al.*, 2002]. On one hand, water table depths may be affected by climate change through altering the partitioning of regional hydrologic components such as runoff, soil moisture storage and lake levels, etc.; on the other hand, large-scale variations of shallow water table depths result in variations of horizontal and vertical distributions of soil moisture [*Chen and Hu*, 2004], which are responsible for the adjustments in the fluxes of heat and moisture between the land surface and the overlying atmosphere. Such adjustments will have impact on precipitation directly through convection or indirectly through advection. In addition, studies have shown that simulated monthly to seasonal mean precipitation is sensitive to initial soil moisture over midlatitude continents because of the long-term memory of soil moisture [*Schär et al.*, 1999; *Koster et al.*, 2000, 2003; *Koster and Suarez*, 2001; *Georgescu et al.*, 2003], thus we can expect that incorporating water table dynamics in a climate model will increase the memory of soil and enhance the seasonal forecast skill because of the long memory of the groundwater. Therefore, understanding the feedback between aquifer and atmosphere at seasonal and interannual scales is needed [*York et al.*, 2002].

[3] With the increasing recognition of the importance of aquifer-atmosphere interaction, dynamical representations of water table in land surface models (LSMs) have been accounted for in several studies. *Liang et al.* [2003] established a dynamic groundwater parameterization for the Variable Infiltration Capacity (VIC) model through reducing it to a moving boundary problem, and solved it by using the

[1]Institute of Atmospheric Physics, Chinese Academy of Sciences, Beijing, China.
[2]Department of Geological Sciences, University of Texas, Austin, Texas, USA.

mass-lumped finite element method [*Xie et al.*, 1998, 1999]. Results indicated that the bottom soil layer was wetter with the new parameterization because of the interaction between unsaturated zone and groundwater. *Yang and Xie* [2003] reduced the moving boundary problem described above to a fixed boundary problem through a coordinate transformation, and the computation cost for the groundwater model was reduced. *Maxwell and Miller* [2005] coupled the Common Land Model (CLM) with the groundwater model ParFlow, which improved the simulation of runoff and soil moisture and demonstrated the need for better groundwater representation in land surface schemes. *Yeh and Eltahir* [2005a, 2005b] demonstrated the critical importance of the presence of shallow water table in affecting the near-surface soil moisture and hence the hydrological processes associated with the soil wetness condition through observations and model experiment in Illinois, and discussed the effect of subgrid variability of water table depth in the grid-scale subsurface runoff. *Niu et al.* [2007] developed a simple groundwater model (SIMGM) by adding an underlying unconfined aquifer to a LSM's soil column, and found that SIMGM produced much wetter soil profiles globally and up to 16% more annual evapotranspiration (ET) than original LSM which used free drainage as the model's lower boundary condition. Recently, *Fan et al.* [2007] used a two-dimensional groundwater model to construct an equilibrium water table as a result of long-term climatic and geologic forcing. *Miguez-Macho et al.* [2007] implemented this groundwater model into the Regional Atmosphere Modeling System (RAMS). The soil moisture simulated by the new model with a groundwater component was significantly higher in the humid river valleys and coastal regions of the eastern U.S., and in the otherwise arid intermountain valleys of the western U.S.

[4] Besides implementing groundwater component into the LSMs, water table dynamics have also been directly coupled with the atmosphere, such as *Gutowski et al.* [2002] and *York et al.* [2002]. In their studies, a single-column atmospheric model was coupled with a detailed land surface model including groundwater model, and the potential advantage of the coupling between atmosphere and aquifer was demonstrated. Recently, *Anyah et al.* [2008] investigated the role of water table dynamics in controlling soil moisture, ET, and precipitation by using the RAMS-Hydro over North America. They found that although including an explicit water table in a climate model did not always make a large difference in the atmospheric simulation, sometimes it did.

[5] In this study, we implement the groundwater model developed by *Yang and Xie* [2003] into the regional climate model RegCM3, which is named RegCM3_GW, and integrate the RegCM3_GW and RegCM3 over east Asia to investigate potential effects of water table dynamics on regional climate. We will show that including a groundwater component into a regional climate model influences its simulations of soil moisture profile and land surface fluxes, and the overlying large-scale atmospheric processes to some extent. Correspondingly, the modification of the mesoscale land-atmosphere interaction and the macroscale atmospheric processes will change the soil moisture and water table in a regional scale.

[6] The paper is organized as follows: we start by describing the regional climate model, the groundwater model, and the setup of numerical experiments in section 2. Section 3 discusses initialization of soil moisture and water table depths, and the validation of precipitation simulated by two regional climate models with or without groundwater component. The feedbacks between the aquifer and atmosphere are analyzed in section 4. The results of the study are concluded in section 5.

2. Model Description and Setup of Numerical Experiments

2.1. RegCM3

[7] The latest version of the regional climate model developed by the Abdus Salam International Centre for Theoretical Physics (ICTP), named the ICTP Regional Climate Model version 3 (RegCM3), is described by *Pal et al.* [2007]. The dynamical core of RegCM3 is based on the hydrostatic version of the fifth-generation Pennsylvania State University–National Center for Atmospheric Research (PSU-NCAR) Mesoscale Model [*Grell et al.*, 1994]. RegCM3 has many physics packages such as the radiative transfer package [*Kiehl et al.*, 1996], land surface model [*Dickinson et al.*, 1993; *Giorgi et al.*, 2003], planetary boundary layer scheme [*Holtslag and Boville*, 1993], ocean flux parameterization [*Zeng et al.*, 1998], lake model [*Hostetler et al.*, 1993], aerosol scheme, and dust parameterizations, etc. The formation of precipitation in RegCM3 is represented in two forms: large-scale precipitation [*Pal et al.*, 2000] and convective precipitation (P_{con}). Three options are available in RegCM3 to represent cumulus convection: the Kuo scheme [*Anthes et al.*, 1987; *Giorgi*, 1991], the Grell scheme [*Grell*, 1993], and the MIT-Emanuel scheme [*Emanuel and Zivkovic-Rothman*, 1999]. RegCM3 has been run over various regions at grid spacings ranging from 10 to 100 km and simulation periods from days to decades to study scientific problems such as future climate change, air quality, water resources, extreme events, agriculture, land cover change, and biosphere-atmosphere interactions, etc. [*Pal et al.*, 2007].

2.2. Groundwater Model

[8] The groundwater model used in this study is based on the parameterization established by *Liang et al.* [2003] and the coordinate transformation developed by *Yang and Xie* [2003]. To have this paper self-contained, relevant main formulations for the water table are briefly summarized as follows:

$$\begin{cases} \dfrac{\partial \theta}{\partial t} = \dfrac{\partial}{\partial z}\left(D(\theta)\dfrac{\partial \theta}{\partial z} - K(\theta)\right) - S(z,t), \\[2mm] \left[K(\theta) - D(\theta)\dfrac{\partial \theta}{\partial z}\right]\bigg|_{z=0} = q_0(t), \\[2mm] \theta(z,t)|_{z=\alpha(t)} = \theta_s, \\[2mm] \theta(z,0) = \theta_0(z)(0 \leq z \leq \alpha(t)), \\[2mm] \left[K(\theta) - D(\theta)\dfrac{\partial \theta}{\partial z}\right]\bigg|_{z=\alpha(t)} = Q_b(t) + E_2(t) - n_e(t)\dfrac{d\alpha}{dt}, \end{cases} \quad (1)$$

where θ is the volumetric soil moisture content [L^3/L^3], $D(\theta)$ is the hydraulic diffusivity [L^2/T], $K(\theta)$ is the hydraulic

conductivity [L/T], $S(z, t)$ is the sink term related to transpiration from the root region [T^{-1}], $q_0(t)$ is the flux across the land surface [L/T], $\alpha(t)$ is the water table depth [L], θ_s is the soil porosity [L^3/L^3], $\theta_0(z)(0 \leq z \leq \alpha(t))$ is the initial volumetric soil moisture content in the unsaturated zone [L^3/L^3], $Q_b(t)$ is the base flow [L/T], $E_2(t)$ is the transpiration rate from the saturated zone [L/T], and $n_e(t)$ is the effective porosity of the porous media [L/L].

[9] Let $x = \frac{z}{\alpha(t)}$ and $\tau = t$ [*Yang and Xie*, 2003], then equation (1) combined with initial and boundary conditions can be transformed as follows:

$$\begin{cases} \dfrac{\partial \theta}{\partial \tau} - \dfrac{x}{\alpha}\dfrac{d\alpha}{d\tau}\dfrac{\partial \theta}{\partial x} = \dfrac{\partial}{\partial x}\left(\dfrac{D(\theta)}{\alpha^2}\dfrac{\partial \theta}{\partial x} - \dfrac{K(\theta)}{\alpha} \right) - S(x, \tau), \\[2mm] \left[K(\theta) - \dfrac{D(\theta)}{\alpha}\dfrac{\partial \theta}{\partial x} \right]\Bigg|_{x=0} = q_0(\tau), \\[2mm] \theta(x, \tau)\Big|_{x=1} = \theta_s, \\[2mm] \theta(x, 0) = \theta_0(x)(0 \leq x \leq 1), \\[2mm] \left[K(\theta) - \dfrac{D(\theta)}{\alpha}\dfrac{\partial \theta}{\partial x} \right]\Bigg|_{x=1} = Q_b(\tau) + E_2(\tau) - n_e(\tau)\dfrac{d\alpha}{d\tau}. \end{cases} \quad (2)$$

Let $\bar{\theta}(\tau) = \int_0^1 \theta(x, \tau)dx$. Integrating the transformed Richards equation (equation (2)) over the interval (0,1), and considering the initial and boundary conditions, it yields

$$\frac{d\alpha}{d\tau} = \frac{\alpha\dfrac{d\bar{\theta}}{d\tau} + Q_b + E_1 + E_2 - q_0}{\theta_s - \bar{\theta} + n_e}, \quad (3)$$

where E_1 is the transpiration rate from the unsaturated zone, and $E_1 = \int_0^{\alpha(t)} S(z, t)dz = \alpha\int_0^1 S(x, \tau)dx$. Therefore, the water table dynamics according to equation (3) can be solved numerically by applying a finite element method in space and a finite difference method in time iteratively [*Liang and Xie*, 2003].

[10] On the basis of the parameterization described above, the groundwater model is coupled with the Biosphere-Atmosphere Transfer Scheme version 1e (BATS1e), which is the land surface component of RegCM3. BATS1e has a vegetation layer, a snow layer, a surface soil layer (10 cm thick), a root zone soil layer (1 m or 1.5 m or 2 m thick), and a total soil layer (3 m thick). The soil water movement formulation of BATS1e is obtained from a multilayer soil model [*Dickinson*, 1984]. While in the coupled model RegCM3_GW, the soil moisture is calculated by using dynamical water table as the lower boundary.

2.3. Setup of Numerical Experiments

[11] The regional climate models RegCM3 and RegCM3_GW are used to conduct the simulations of the regional climate over east Asia during the summertime of 2000, driven by the meteorological initial and boundary conditions from the European Centre for Medium-Range Weather Forecast (ECMWF) 40 year reanalysis data sets. The Grell scheme [*Grell*, 1993] with Fritsch and Chappell closure [*Fritsch and Chappell*, 1980] is adopted as the cumulus convection scheme. The model domain is centered at 102°E, 36°N, with a grid size of 60 km and 120 × 90 grid points. There are 23 vertical levels, and the model top is 50 mbar. The simulations start at 26 May 2000, and end at 31 August 2000. The first 6 days are used as the spin-up time for the atmospheric models.

3. Water Table Depth Initialization and Precipitation Simulation Results

3.1. Initialization of Soil Moisture and Water Table Depths

[12] Because of the availability of observed soil moisture and water table depths [*Yuan et al.*, 2008], the initializations of the land surface variables such as soil moisture, soil temperature and water table depths are carried out by spinning up the offline land surface model BATS_GW and the regional climate model RegCM3_GW. On the basis of the discussion of spin-up processes in the previous studies [*Yang et al.*, 1995; *Cosgrove et al.*, 2003], the equilibrium of the soil moisture and water table depths can be obtained through running the land surface model by using multiyear climate forcing repeatedly. In this study, global forcing data set for 1961–2000 with 3-hourly and T62 resolution [*Qian et al.*, 2006] are merged with daily precipitation observations at over 700 Chinese meteorological stations, and the merged data are interpolated to the regional climate models' horizontal resolution. Then we initialize the BATS_GW with a water table depth of 4 m and run the model for 40 years from 1961 to 2000, and use the prognostic variables at the end of the run as the initial conditions for another 40-year run in each grid cell for the regional climate model. After spinning up the BATS_GW for 200 years to reach equilibrium, we run the land surface model BATS_GW from 1 January 1961 to 31 December 1999 and the regional climate model RegCM3_GW from 1 January 2000 to 25 May 2000. The final spin-up results such as water table depths, soil moisture, ground temperature, temperature of foliage and air temperature within foliage are adopted as the initial land surface conditions for the numerical experiments in this study.

[13] Figure 1 shows the spin-up results for the soil moisture in each soil layer and the water table depths, and the observed top layer soil moisture and shallow water table depths. The soil moisture observations (which are collected every 10 days) are supplied by National Satellite Meteorological Center, China Meteorological Administration. The observed shallow water table depths (which are collected every month) are compiled by *Yuan et al.* [2008]. The spatial pattern for the simulated soil moisture and water table depths are correlated quite well, and different water table depths reflect different climate conditions and land covers reasonably. The water tables are shallower over eastern China, which is a typical monsoon area, and deeper over northwestern China, which is a desert area. The water tables over northern China are deeper than that over southern China and northeastern China. Figures 1a and 1e show that the simulated top layer soil moisture is consistent with station observations, especially for northern China. The simulated water table depths (Figure 1d) over northern and northeastern China agree with station observation (Figure 1f) to some extent. In order to analyze the effects of water table dynamics on regional climate over east Asian monsoon area, we divide the east part of the study domain into four subdomains (Figure 1d). Region 1 is located in northeastern China (42–50°N, 115–125°E), which repre-
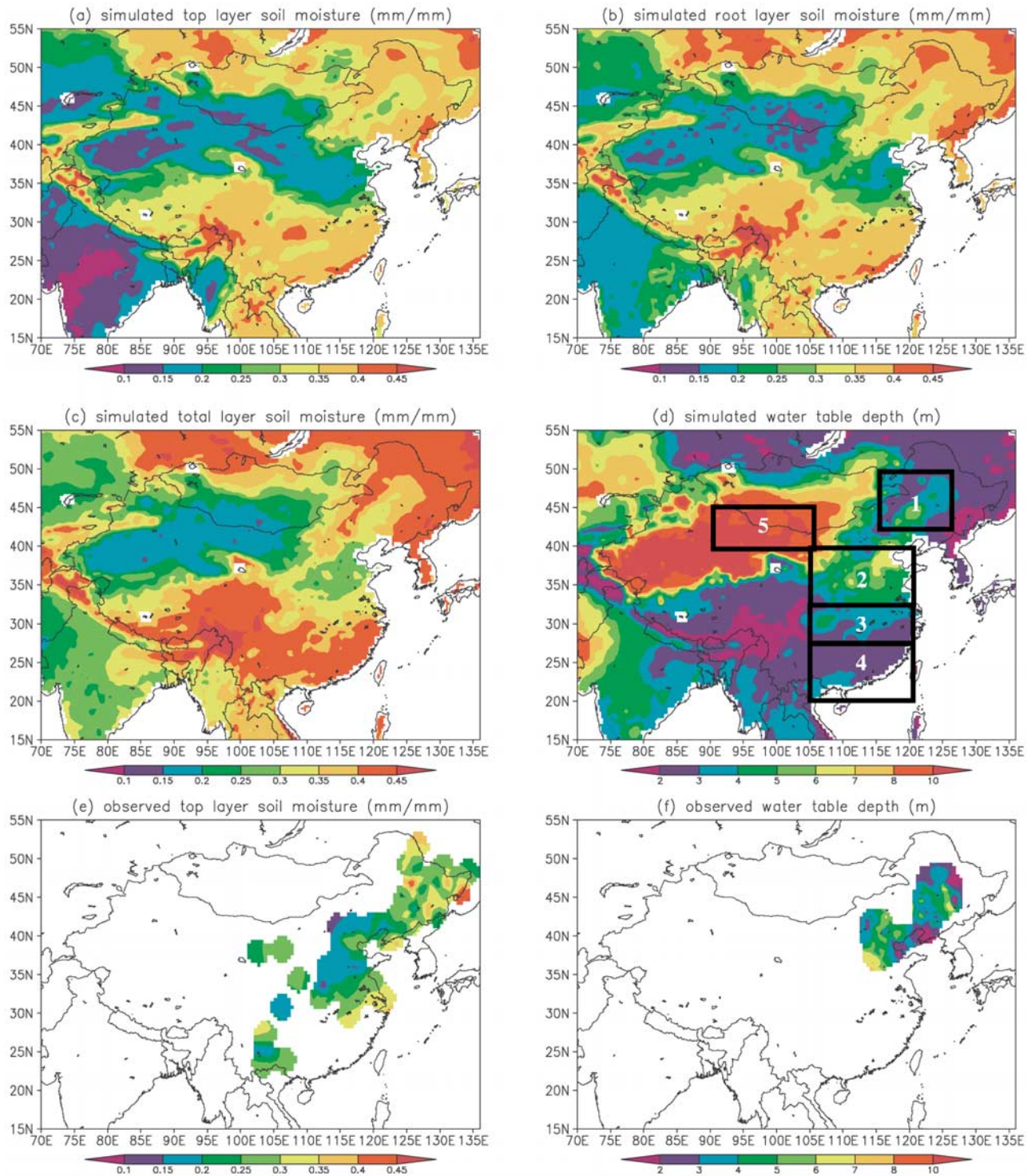
Figure 1. Spin-up results for the soil moisture and water table depths and the observed top layer soil moisture and shallow water table depths. The simulated soil moisture (mm mm^{-1}) for the (a) topsoil layer, (b) root soil layer, and (c) total soil layer; (d) the simulated water table depths (m); (e) the observed top layer soil moisture (mm mm^{-1}); and (f) the observed shallow water table depths (m).
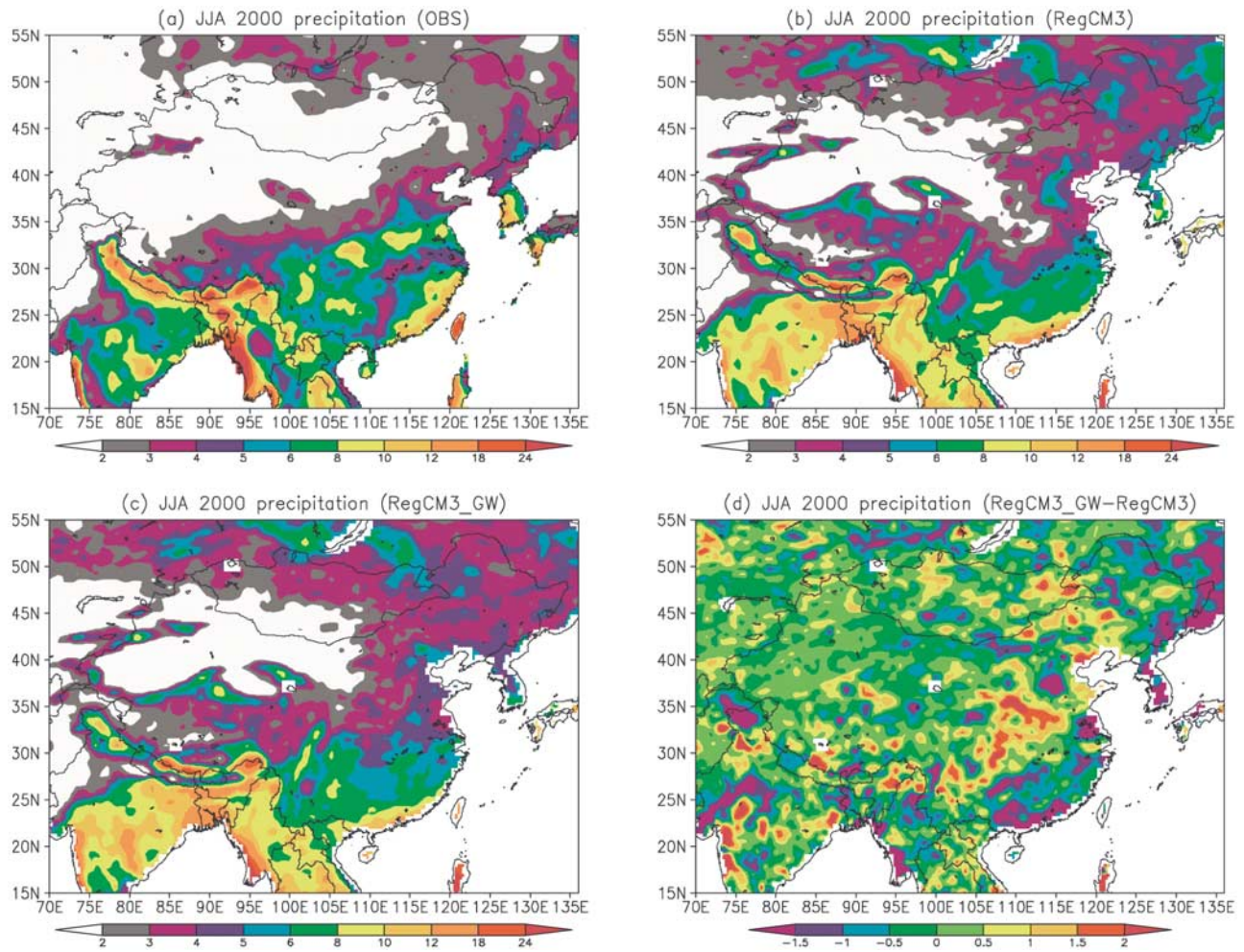
Figure 2. JJA mean precipitation (mm d^{-1}) from (a) observation, (b) RegCM3, (c) RegCM3_GW, and (d) RegCM3_GW minus RegCM3.

sents medium water table depth ($\sim$3 m) and semihumid climate (hereafter referred to as MSH1 region). Region 2 is located in northern China (32–40°N, 105–118°E), which represents deep water table depth ($\sim$4.5 m, deeper than the model's soil column) and semiarid climate (hereafter referred to as DSA2 region). Region 3 is located in the middle and lower reaches of Yangtze River (26–32°N, 105–118°E), which represents medium water table depth ($\sim$2.7 m) and humid climate (hereafter referred to as MHU3 region). Region 4 is located in southern China (20–26°N, 105–118°E), which represents shallow water table depth ($\sim$2.2 m) and humid climate (hereafter referred to as SHU4 region). In addition, we select an arid region (40–45°N, 90–105°E) where the water table is much deeper than the monsoon region for comparison (hereafter referred to as DAR5 region).

3.2. Simulation for Precipitation

[14] The JJA mean precipitation during the summer of 2000 simulated by RegCM3 and RegCM3_GW are compared with observations [*Xie et al.*, 2007], which are shown in Figure 2. During the summer of 2000, the east Asian summer monsoon was active in the south of its normal position, the west Pacific Ocean subtropical high was in the

east and north of its normal position, and the blocking high over Baikal was stable. Therefore, the main rain belt was located in the Huang-Huai river basin, and the southeast and southwest of China, while there was a drought in northern China. Figure 2 shows that the spatial distributions of total precipitation simulated by RegCM3 and RegCM3_GW agree with observations to some extent. Although neither of the models captures the main rain belt located in the Huang-Huai river basin, the RegCM3_GW alleviates this underestimation obviously. The RegCM3_GW also reduces the overestimation of precipitation over southern China as well (Figure 2d).

[15] Figure 3 shows the simulated and observed monthly mean precipitation and daily precipitation averaged over the subdomains, and Table 1 lists the detailed statistics for the daily series. Both of the models overestimate precipitation over MSH1, SHU4 and DAR5 regions, and underestimate it over DSA2 and MHU3 regions. All of the correlation coefficients (CC) between the simulations and observations satisfy the 95% confidence level (0.205), and the highest CC for the two models occurs in DSA2 region. The RegCM3_GW has a better performance than RegCM3 over DSA2, SHU4 and DAR5 regions (Figures 3b, 3d, and 3e) with respect to the
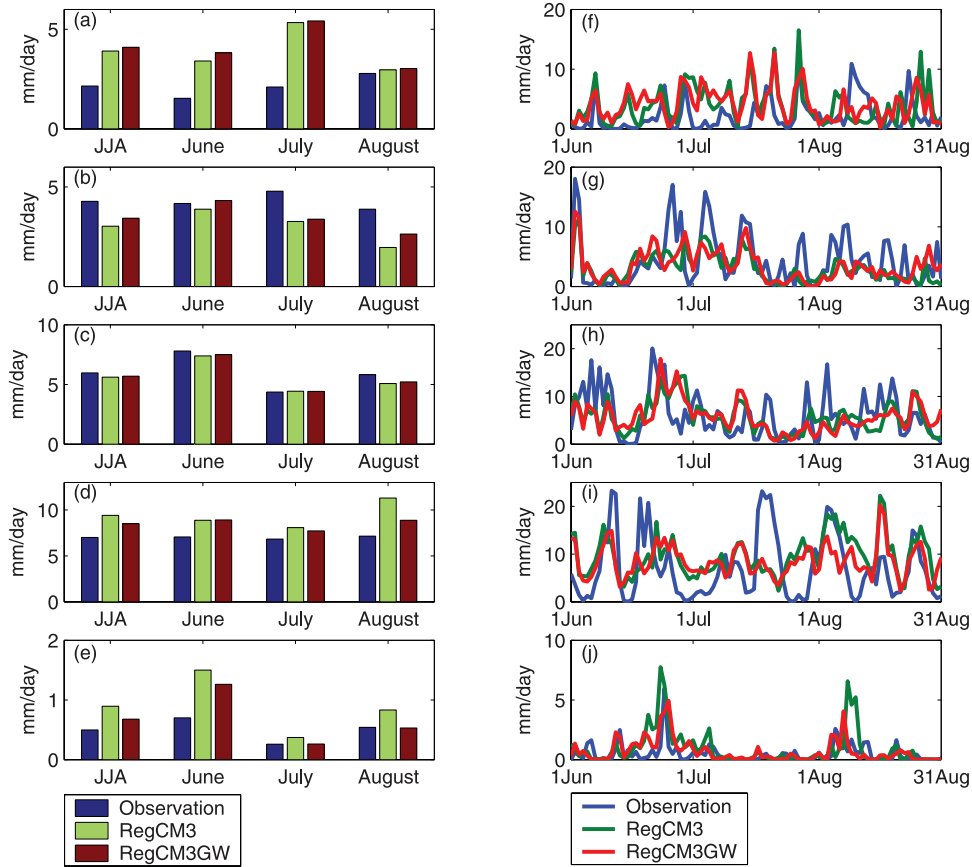
Figure 3. Simulated and observed (a–e) monthly mean precipitation (mm d^{-1}) and (f–j) daily precipitation (mm d^{-1}) averaged over the subdomains shown in Figure 1d. Figures 3a and 3f, 3b and 3g, 3c and 3h, 3d and 3i, and 3e and 3j show the results for regions MSH1, DSA2, MHU3, SHU4 and DAR5, respectively.

systematic error (*ME*). The relative variations of *ME* calculated by $\dfrac{|ME_{\text{RegCM3\_GW}}| - |ME_{\text{RegCM3}}|}{|ME_{\text{RegCM3}}|} \times 100\%$ over the five regions are 5.6%, −38.5%, −25%, −39.8% and −50% respectively (Table 1). However, there are not significant improvements with respect to the mean absolute error (MAE) and the root mean squared error (RMSE).

4. Feedbacks Between Aquifer and Atmosphere

[16] In this section, we will analyze the physical processes that are responsible for the simulated aquifer-atmosphere feedbacks.

4.1. Effects of Water Table Dynamics on Local Land Surface Conditions

[17] To detect the underlying mechanisms of the interactions between the aquifer and atmosphere, we begin by discussing the differences of the simulated land surface variables induced by water table dynamics.

[18] The detailed differences in land surface water and energy variables averaged over the subdomains are listed in Table 2. First of all, we analyze the differences in soil moisture and their impacts on ground evaporation and transpiration. Figure 4 shows the areal averaged daily time series of soil moisture for the top and root soil layers, total runoff and water table depths simulated by regional climate

Table 1. Statistics of the Daily Precipitation Series Simulated by the Two Models[a]

	ME (mm d^{-1})		MAE (mm d^{-1})		RMSE (mm d^{-1})		CC	
	RCM	RCM_GW	RCM	RCM_GW	RCM	RCM_GW	RCM	RCM_GW
MSH1	1.8	1.9	2.9	3.1	4.0	3.9	0.22	0.21
DSA2	−1.3	−0.8	2.7	2.6	3.7	3.6	0.58	0.61
MHU3	−0.4	−0.3	3.8	3.4	4.8	4.6	0.29	0.37
SHU4	2.4	1.5	5.8	5.7	7.1	6.8	0.24	0.30
DAR5	0.4	0.2	0.8	0.6	1.4	0.9	0.45	0.52

[a]ME is the systematic error, MAE is the mean absolute error, RMSE is the root mean squared error, and CC is the correlation coefficient. RCM and RCM_GW denote the results from RegCM3 and RegCM3_GW, respectively.

Table 2. Differences (RegCM3_GW Minus RegCM3) in Land Surface Water and Energy Variables Averaged Over the Subdomains

	MSH1	DSA2	MHU3	SHU4	DAR5
JJA Differences in Water Variables					
Top layer soil moisture (mm mm^{-1})	0.033	0.010	0.019	0.010	0.006
Root layer soil moisture (mm mm^{-1})	0.009	0.012	0.012	0.010	−0.011
2-m specific humidity (g kg^{-1})	0.337	0.714	−0.067	−0.089	0.073
Total evapotranspiration (mm d^{-1})	−0.040	0.433	−0.003	0.033	−0.083
Canopy evaporation (mm d^{-1})	0.092	0.216	0.060	0.048	−0.005
Ground evaporation (mm d^{-1})	0.022	0.124	0.042	0.007	−0.045
Transpiration (mm d^{-1})	−0.153	0.093	−0.104	−0.022	−0.033
Convective precipitation (mm d^{-1})	0.259	0.682	−0.080	−1.890	−0.149
Total precipitation (mm d^{-1})	0.187	0.406	0.076	−0.921	−0.216
JJA Differences in Energy Variables					
Ground temperature (K)	−0.140	−1.166	−0.366	−0.076	0.285
2-m temperature (K)	−0.093	−0.967	−0.262	−0.106	0.180
Net absorbed shortwave (W m^{-2})	−10.402	−8.465	−5.516	0.937	−0.591
Net longwave (W m^{-2})	−6.024	−8.533	−2.725	−0.403	−0.616
Sensible heat (W m^{-2})	−3.842	−12.361	−2.700	0.280	1.598
Latent heat (W m^{-2})	−1.149	12.542	−0.093	0.965	−2.389

models. Compared with the observations and ECMWF reanalysis, the regional climate model can roughly capture the variability of soil moisture, runoff and water table depth. The variations of soil moisture for top layer simulated by RegCM3_GW are smaller than that by RegCM3, especially for humid regions (Figures 4a, 4e, 4i, 4m, and 4q). The topsoil layers become wetter over the four regions in the monsoon area, which enhance the ground evaporation. The most obvious increase in ground evaporation occurs in semiarid region (~0.124 mm d^{-1}, see Table 2). The root zone soil layers also become wetter over the monsoon area, but only increase the transpiration over semiarid region. In fact, the soil water is the key factor in the areas where there is not enough water for the transpiration, which is parameterized as the maximum transpiration available from the vegetation in BATS1e [*Dickinson et al.*, 1993]. However, in the areas where soil water is not the limiting factor for transpiration, such as humid areas (regions MHU3 and SHU4), the transpiration only depends on the climate and vegetation conditions such as unwetted fraction of leaf-stem area free to transpire, solar radiation, temperature, vapor pressure deficit, and wind, etc. Table 2 also shows that the increase of canopy evaporation over semiarid region is more obvious than that over humid and semihumid regions.

[19] The differences in ground evaporation, transpiration and canopy evaporation constitute the differences in ET, and the diurnal cycles of ET are shown in Figures 5a, 5e, 5i, 5m, and 5q. The largest increase of ET occurs over semiarid region (~0.433 mm d^{-1}), and the maximum difference occurs around 1400 local time when the ET reaches its peak value. Although the climate model has deficiencies in capturing the broad pattern of the diurnal cycle of precipitation [*Dai et al.*, 1999], we plot the diurnal cycle of P_{con} simulated by two models for comparison (Figures 5b, 5f, 5j, 5n, and 5r). Corresponding to the difference in the diurnal cycle of ET, the largest difference in the diurnal cycle of P_{con} also occurs in DSA2 region. But the relation between the ET and P_{con} is very complicated. The higher ET corresponds to higher P_{con} over DSA2 region, but in the MSH1 region, the ET decreases while P_{con} increases. One of the possible reasons for the reduced ET and enhanced

P_{con} over MSH1 region is related to the atmospheric humidity difference (Figures 5c, 5g, 5k, 5o, and 5s). In fact, Figures 5a and 5c show that although the ET decreases slightly (−0.04 mm d^{-1}), the 2-m specific humidity does increase (because of the large-scale horizontal moisture convergence), thus the air becomes wetter (0.337 g kg^{-1}) and the P_{con} increases (0.259 mm d^{-1}). Figures 5d, 5h, 5l, 5p, and 5t show that the variations of the diurnal cycle differences for surface energy components are larger over semiarid region (the mean reduction of sensible heat can reach ~46 W m^{-2} at noon) than that over humid region. From the above analysis, it is found that the shallow water table dynamics (shallower than 8−10 m) will make the model simulate wetter soil, higher ET and P_{con} over semiarid region in the monsoon area. However, the water table dynamics does not have direct impact on regional climate over the arid region where water table is deep (deeper than 10 m), such as the DAR5 region in this study.

[20] The variations of land surface water and energy variables described above will influence the structure of the boundary layer. Therefore, we plot the July mean diurnal evolution of vertical profiles of pseudoequivalent potential temperature θ_{se} averaged over the subdomains in Figure 6. The profile of pseudoequivalent potential temperature can be viewed as the most important aspect of the thermodynamic stratification, and it is directly related to convective instability. The most obvious differences of the profile for the pseudoequivalent potential temperature occur in semiarid region (Figure 6b). The RegCM3_GW produces a larger vertical decreasing rate ($\partial\theta_{se}/\partial p$) than the RegCM3 over DSA2 region, which contributes to higher potential for convective instability. The release of this instability is facilitated by lowering the level of free convection (the mean reduction of planetary boundary layer height is 73.9 m over DSA2 region), which is promoted by the moistening of the boundary layer.

4.2. Coupling Between the Local Aquifer-Atmosphere Interaction and the Macroscale Atmospheric Processes

[21] The differences in land surface variables and boundary structure described above can explain the effects of water
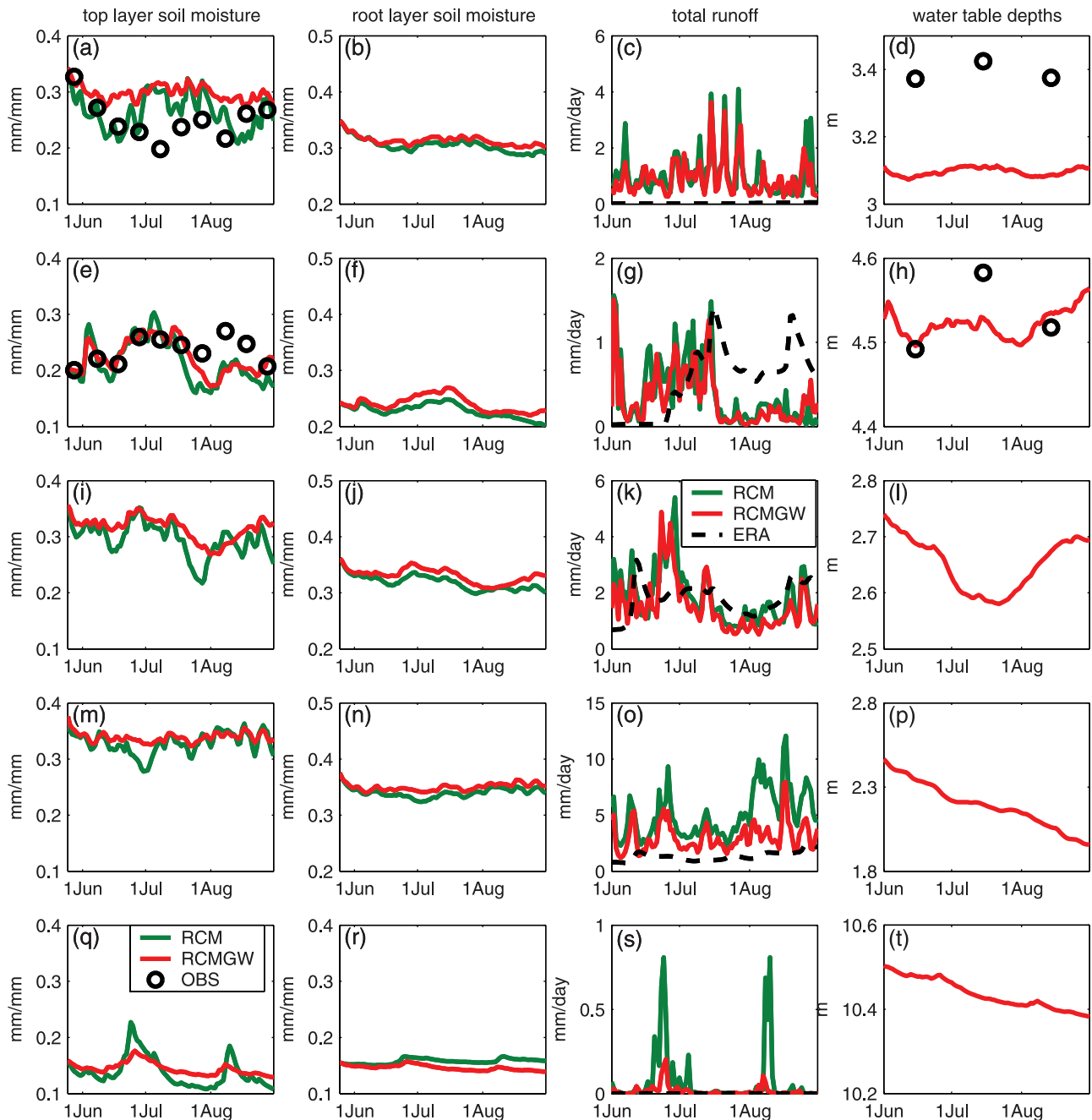
Figure 4. Daily time series for regions (a–d) MSH1, (e–h) DSA2, (i–l) MHU3, (m–p) SHU4, and (q–t) DAR5 of the simulated and observed soil moisture for the topsoil layer (Figures 4a, 4e, 4i, 4m, and 4q) and root soil layer (Figures 4b, 4f, 4j, 4n, and 4r), total runoff (Figures 4c, 4g, 4k, 4o, and 4s) and water table depths (Figures 4d, 4h, 4l, 4p, and 4t) averaged over the subdomains. The soil moisture and water table depths are observed every 10 days and every month, respectively.

table dynamics on regional climate from the local recycling aspect. However, the large-scale variations of water table will change the spatial distribution of soil moisture and surface fluxes, and consequently influence the overlying atmospheric circulation, which will redistribute the water and energy through advection. Figure 7 shows the spatial differences (RegCM3_GW minus RegCM3) in JJA mean soil moisture of root soil layer (RSW), ET, P_{con}, 500 hPa geopotential height and 850 hPa wind. Although the RSW increase in

most parts of eastern China, the ET and P_{con} only increase obviously over semiarid region. The opposite variations of ET and P_{con} over northeastern and southern China can be explained by the difference in circulation (Figure 7d). There is a positive anomaly center of 500 hPa geopotential height located at northeastern China due to the advection and heating effect of condensation (the JJA mean 500 hPa air temperature simulated by RegCM3_GW is 0.5°C higher than that by RegCM3 over northeastern China), which
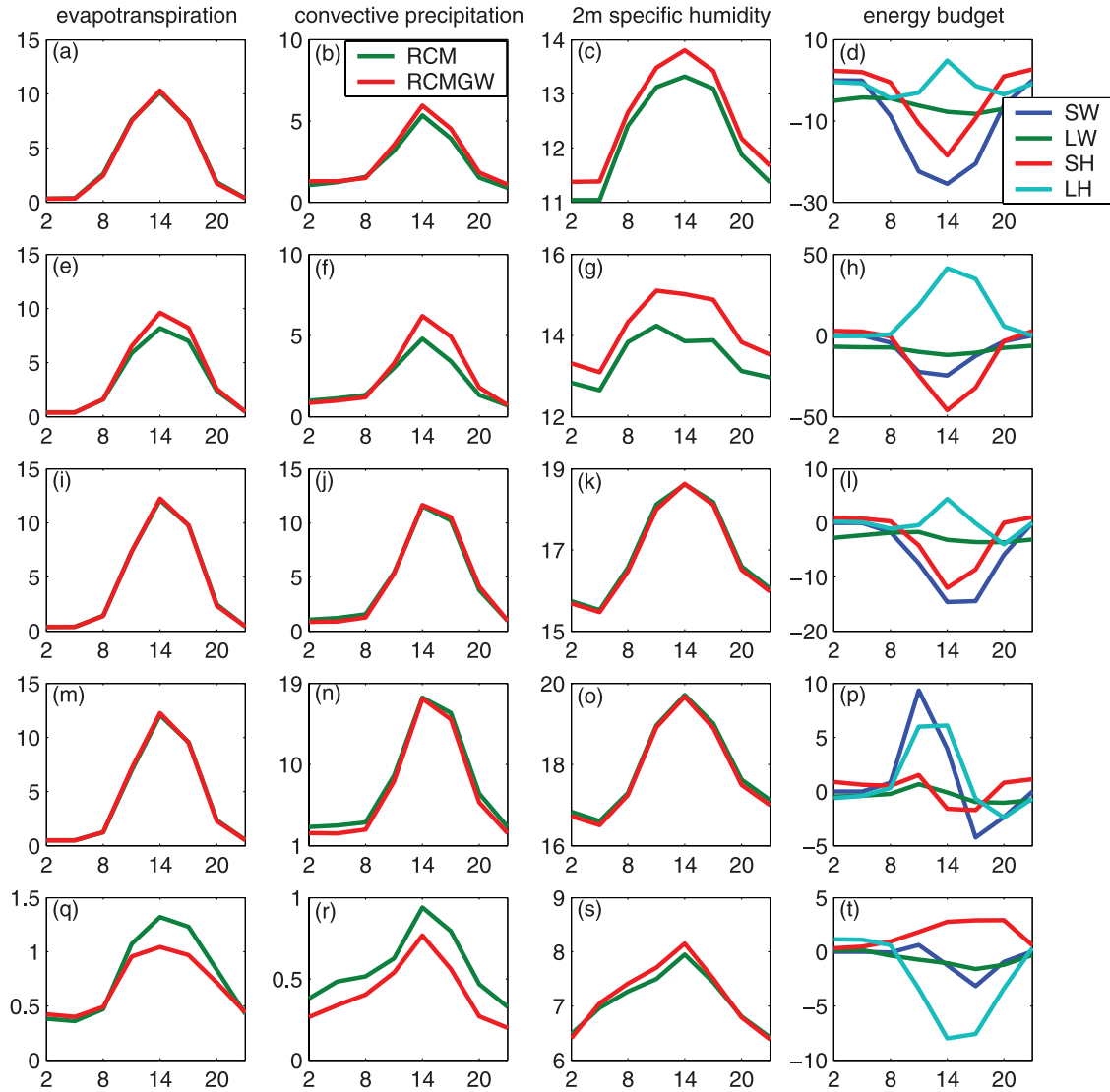
Figure 5. JJA mean diurnal cycle for regions (a−d) MSH1, (e−h) DSA2, (i−l) MHU3, (m−p) SHU4, and (q−t) DAR5 of evapotranspiration (Figures 5a, 5e, 5i, 5m, and 5q, mm d^{-1}), convective precipitation (Figures 5b, 5f, 5j, 5n, and 5r, mm d^{-1}), 2-m specific humidity (Figures 5c, 5g, 5k, 5o, and 5s, g kg^{-1}), and differences in energy components (Figures 5d, 5h, 5l, 5p, and 5t, W m^{-2}) averaged over the subdomains. SW, LW, SH, and LH in Figures 5d, 5h, 5l, 5p, and 5t denote differences in net absorbed shortwave, net longwave, sensible heat, and latent heat, respectively. Horizontal axes are local time.

enhances the westerly wind over the north part of the anomaly center and weaken it over the south part. The 850 hPa wind difference indicates that there is a distinct circulation anomaly along the coastline and across southern China. The changes of circulation affect the water vapor transport and result in a moisture convergence tendency over MSH1 region and a moisture divergence tendency over SHU4 region. The atmospheric moisture convergence and divergence lead to the increase and decrease of P_{con} over MSH1 region and SHU4 region, respectively.

[22] In order to compare the effects of the macroscale atmospheric processes and mesoscale land-atmosphere interactions on the development of precipitation in details, the atmospheric moisture budgets are analyzed in each subdomain. Following the definitions given by *Schär et al.*

[1999], the balance equation for the atmospheric moisture can be written as

$$\Delta W = q_{in} - q_{out} + ET_b - P_b, \qquad (4)$$

where ΔW (mm d^{-1}) denotes the tendency of the atmospheric water content during the integration period; q_{in} (mm d^{-1}) and q_{out} (mm d^{-1}) denote the JJA mean water flux into and out of the domain, respectively; ET_b and P_b are the JJA mean evapotranspiration and precipitation averaged in each domain, respectively. The q_{in} and q_{out} are corrected by residual water. The moisture convergence (MC = q_{in} − q_{out}) calculated in each subdomain are listed in Table 3 (note that the ET_b and P_b are slightly different from Table 2 because of the consideration of ocean grid cells). The MC simulated by RegCM3_GW is more than that by RegCM3
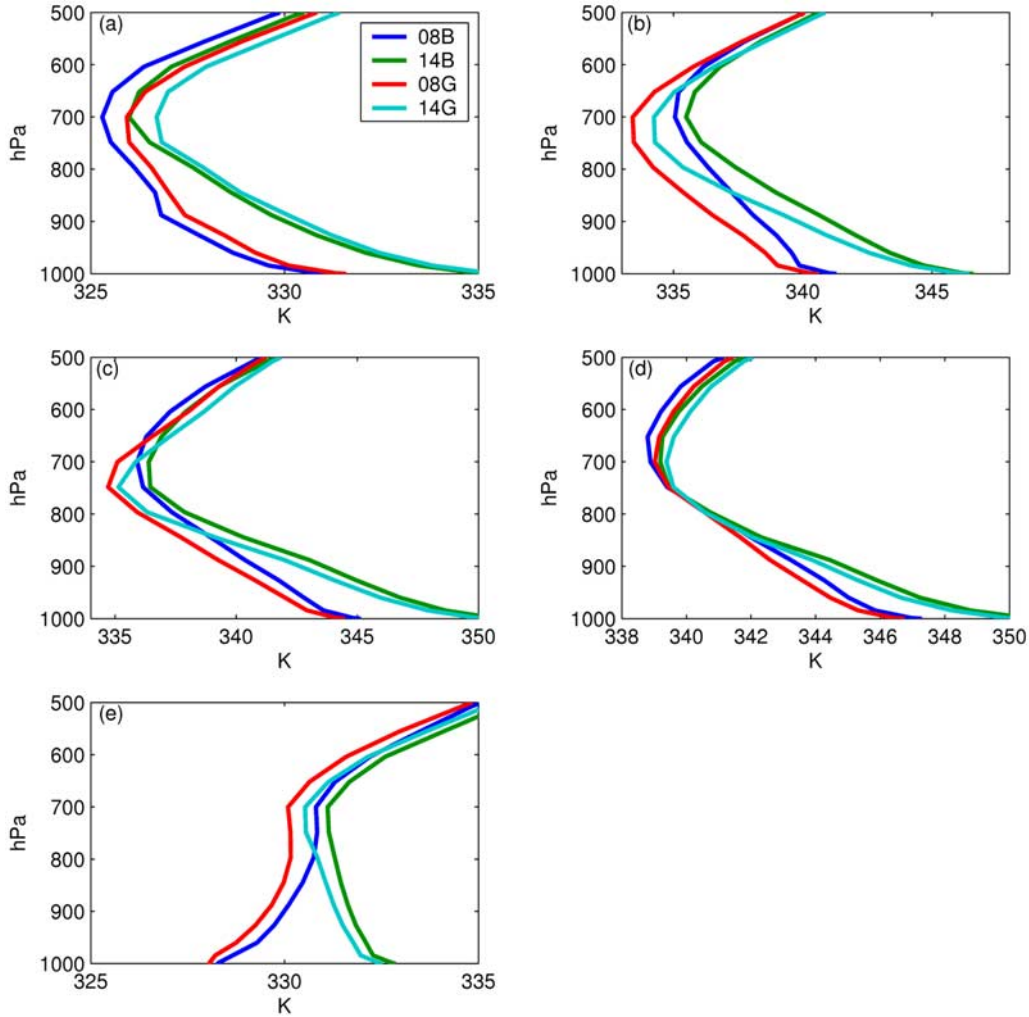
Figure 6. July mean diurnal evolution of vertical profiles of pseudoequivalent potential temperature θ_{se} averaged over the subdomains. Results are shown for RegCM3 (B) and RegCM3_GW (G) and for the local times 0800 (08) and 1400 (14), respectively.

over MSH1 region, which leads to more precipitation, although the ET simulated by RegCM3_GW is slightly less than that by RegCM3 over this region. The MC simulated by RegCM3_GW is less than that by RegCM3 over SHU4 region, and leads to the decrease of precipitation. Figure 8 shows the water budget calculated separately over each subdomain for RegCM3 and RegCM3_GW. Corresponding to the analysis of circulation change (Figure 7d), the zonal moisture flux increases over MSH1 and DAR5 regions, and decreases over DSA2 and SHU4 regions, while the meridional moisture flux increases over MSH1 and DSA2 regions and decreases over SHU4 region, respectively. Specifically, the directions of the zonal moisture flux over the eastern boundary of MHU3 region are opposite for the two regional models. The incoming moisture fluxes at the southern and western boundaries of MSH1 region increase by 240% and 27% respectively, which contributes to the increase of MC from 0.15 mm d^{-1} to 0.44 mm d^{-1}. The incoming moisture fluxes at the southern and western boundaries of SHU4 region decrease by 18% and 20% respectively, which contributes to the decrease of MC from 6.33 mm d^{-1} to 5.71 mm d^{-1}.

[23] We use two indices to analyze the water cycle over each subdomain. The recycling rate β is defined as the fraction of precipitation in a certain analysis domain that originates from ET within the same domain, and the precipitation efficiency χ describes the fraction of water that enters the domain (either by ET or atmospheric transport) and subsequently falls as precipitation within it [*Schär et al.*, 1999]:

$$\beta = \mathrm{ET_b}/(\mathrm{q_{in}} + \mathrm{ET_b}), \qquad (5)$$

$$\chi = \mathrm{P_b}/(\mathrm{q_{in}} + \mathrm{ET_b}). \qquad (6)$$

[24] Table 3 shows that besides the arid region, the smallest recycling rate β and the largest precipitation efficiency χ both occur over SHU4 region, which indicates the ambient flow has strong control on the development of the precipitation over this region. As the water table dynamics is considered in the regional climate model, the recycling rate and precipitation efficiency over DSA2 region increase by 15.1% and 15.3%, respectively. Further-
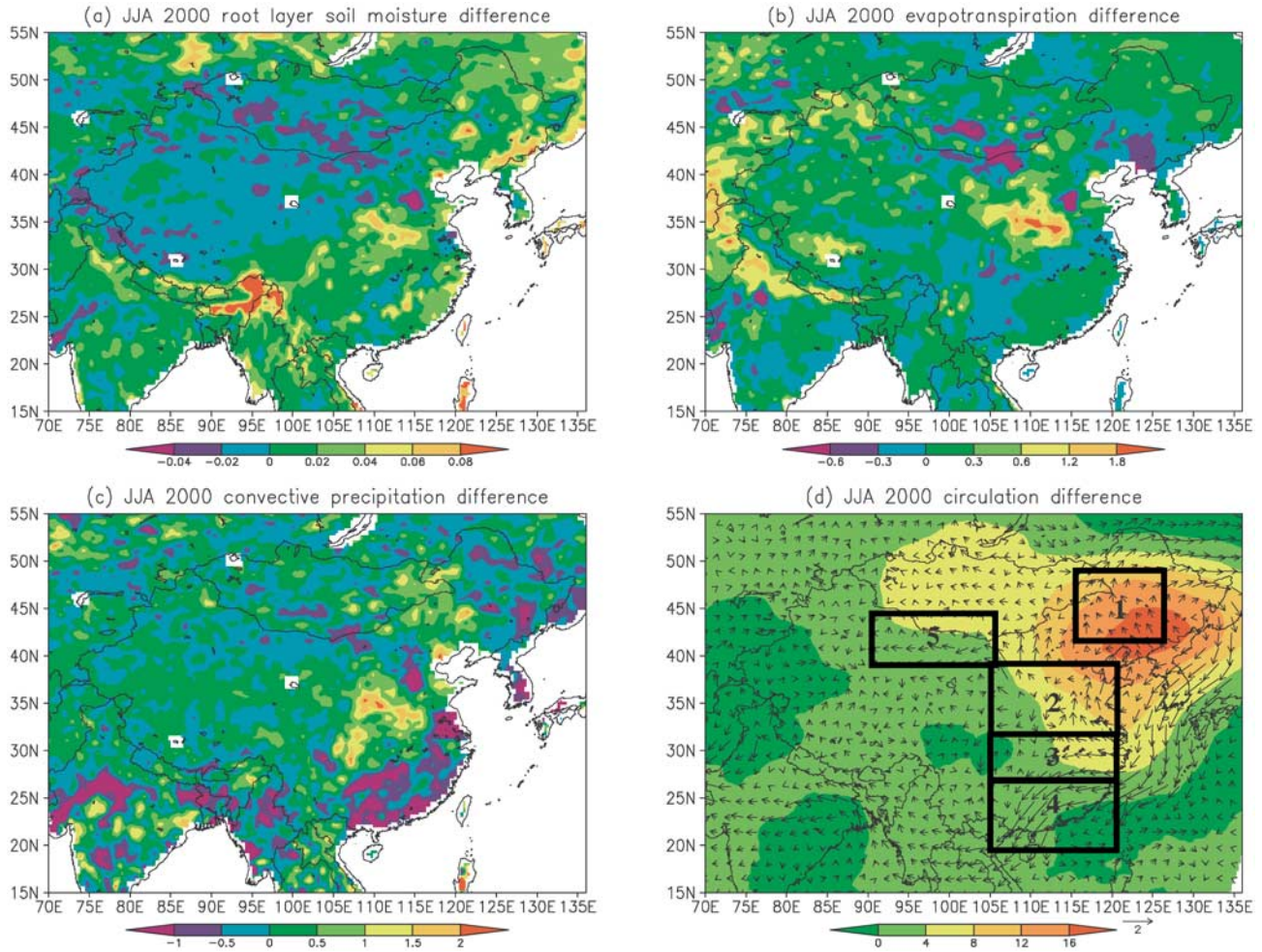
Figure 7. JJA mean differences (RegCM3_GW minus RegCM3) in (a) soil moisture for root soil layer (mm mm^{-1}), (b) evapotranspiration (mm d^{-1}), (c) convective precipitation (mm d^{-1}), and (d) 500 hPa geopotential height (gpm) and 850 hPa wind (m s^{-1}).

more, the precipitation efficiencies increase by 0.9% and 4.4% over MSH1 and MHU3 regions respectively, while decreasing by 2.1% over SHU4 region.

4.3. Sensitivity of Aquifer-Atmosphere Interactions to a Change in Convection Scheme

[25] Because all of the analyses discussed above are based on one convection scheme, the Grell scheme [*Grell*, 1993] with Fritsch and Chappell closure, it is important to

ascertain whether the results are sensitive to the changes of convection parameterizations. Therefore, we select the Kuo scheme [*Anthes et al.*, 1987] and carry out the same experiments described above to analyze the aquifer-atmosphere interactions.

[26] The Kuo scheme does not explicitly account for the downdraft circulation, and the precipitation is initiated when the moisture convergence in a column exceeds a given threshold and the vertical sounding is unstable, while the

Table 3. Atmospheric Water Balance Components and Two Water Cycle Indices Averaged Over the Subdomains

	MSH1		DSA2		MHU3		SHU4		DAR5	
	RCM	RCMGW	RCM	RCMGW	RCM	RCMGW	RCM	RCMGW	RCM	RCMGW
ET$_b$ (mm d^{-1})	3.85	3.82	3.27	3.70	4.28	4.28	4.50	4.52	0.82	0.74
P$_b$ (mm d^{-1})	3.91	4.09	3.02	3.43	5.44	5.56	10.90	10.20	0.95	0.75
q$_{in}$ (mm d^{-1})	32.16	33.50	27.54	26.62	35.83	34.95	51.43	48.84	20.55	20.58
q$_{out}$ (mm d^{-1})	32.01	33.06	27.71	26.69	34.70	33.55	45.10	43.13	20.37	20.51
MC (mm d^{-1})	0.15	0.44	−0.17	−0.07	1.13	1.40	6.33	5.71	0.18	0.07
β (%)	10.7	10.2	10.6	12.2	10.7	10.9	8.1	8.5	3.8	3.5
χ (%)	10.9	11.0	9.8	11.3	13.6	14.2	19.5	19.1	4.5	3.5
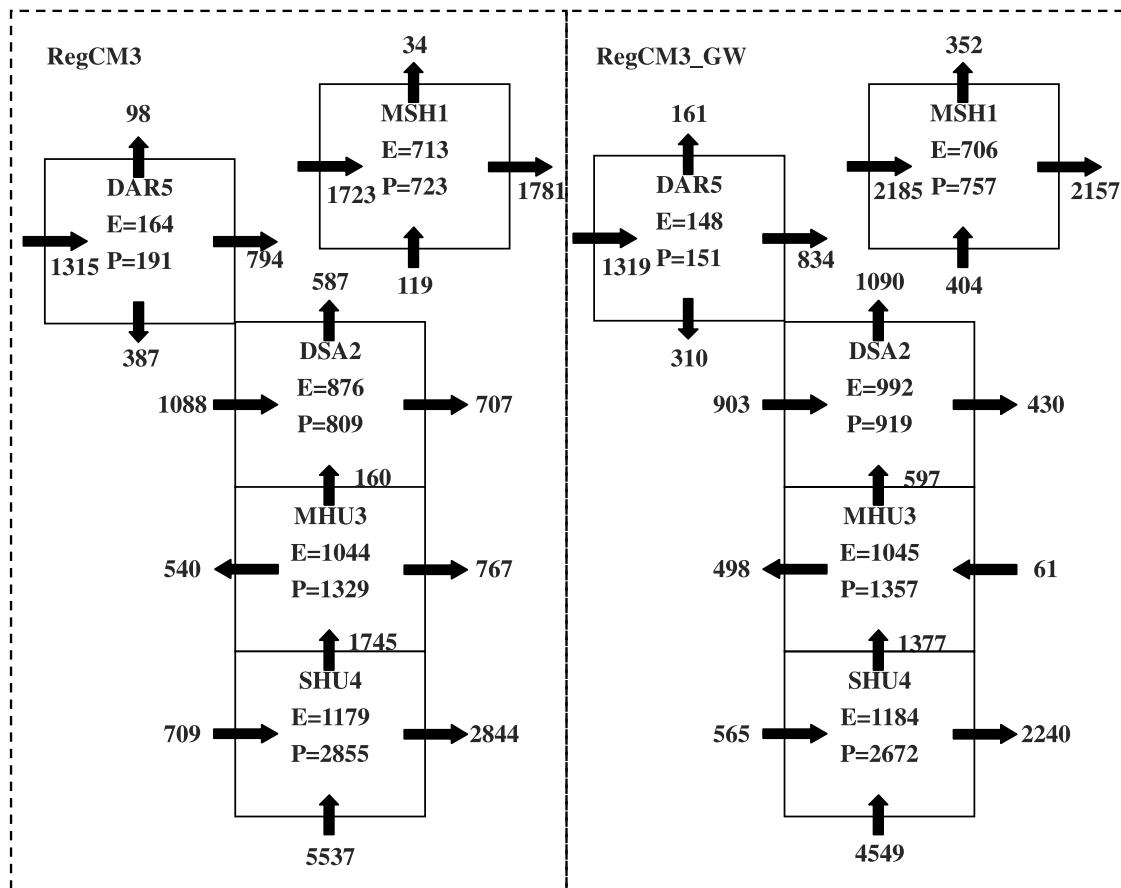
Figure 8. Atmospheric water budget diagram for (left) RegCM3 and (right) RegCM3_GW. E and P stand for evaporation and precipitation, respectively. Arrows indicate incoming and outgoing zonal and meridional moisture fluxes, respectively. Each numeral denote the total amount for all the grid cells within the subdomains, and units are mm d^{-1}.

Grell scheme explicitly considers clouds as two steady state circulations: an updraft and a downdraft [*Dai et al.*, 1999]. Figure 9 shows the daily time series of differences in P_{con} based on two cumulus convection schemes averaged over the subdomains. The standard deviations of difference series for P_{con} based on Grell scheme are less than that based on Kuo scheme, and the percentages of the decrease of standard deviation over the four monsoon regions are 58%, 39%, 23%, and 46%, respectively. Therefore, the effects of water table dynamics on the simulated P_{con} are stronger for the Kuo scheme than that for the Grell scheme over the monsoon area, which is similar to the results of the influences of cumulus schemes on the response of rainfall to soil moisture described by *Pan et al.* [1996]. Figure 10 shows that the recycling rate and precipitation efficiency for the experiments based on the Grell scheme are larger than that based on the Kuo scheme, but the variations of recycling rate and precipitation efficiency simulated by the two cumulus convection schemes are similar, though there are opposite variations of recycling rate over regions MSH1, SHU4 and DAR5 (Figure 10a) where the variations of large-scale circulation control the feedback between the aquifer and atmosphere. Figure 10 also indicates that the simulated recycling rate and precipitation efficiency are more sensitive to the convection scheme than to the inclusion of water table dynamics, especially for the humid regions where the convection is active and model predictive skill is low. Therefore, the cumulus parameterization is still a major uncertainty for regional climate simulation, and perhaps the optimal ensemble of multiple cumulus schemes can reduce the uncertainty [*Liang et al.*, 2007].

[27] Although the model is sensitive to the convection scheme, the differences in soil moisture and ET's components simulated by Kuo scheme are consistent with that by Grell scheme. For example, in the Kuo scheme, the topsoil layers also become wetter over each subdomain as the water table dynamics considered, which also enhance the bare soil evaporation. And the root zone soil layers also become wetter over the four monsoon regions, but only lead to the increase of transpiration over DSA2 region.

[28] To conclude the analysis of mechanism for the aquifer-atmosphere interaction, the schematic chart is shown in Figure 11. The interaction between the groundwater and atmosphere consists of a local water cycle and a large-scale water cycle. On one hand, the local variations of water table change the vertical profiles of soil moisture, and affect the partitioning of available energy at the ground surface into sensible and latent heat, and thus influence the
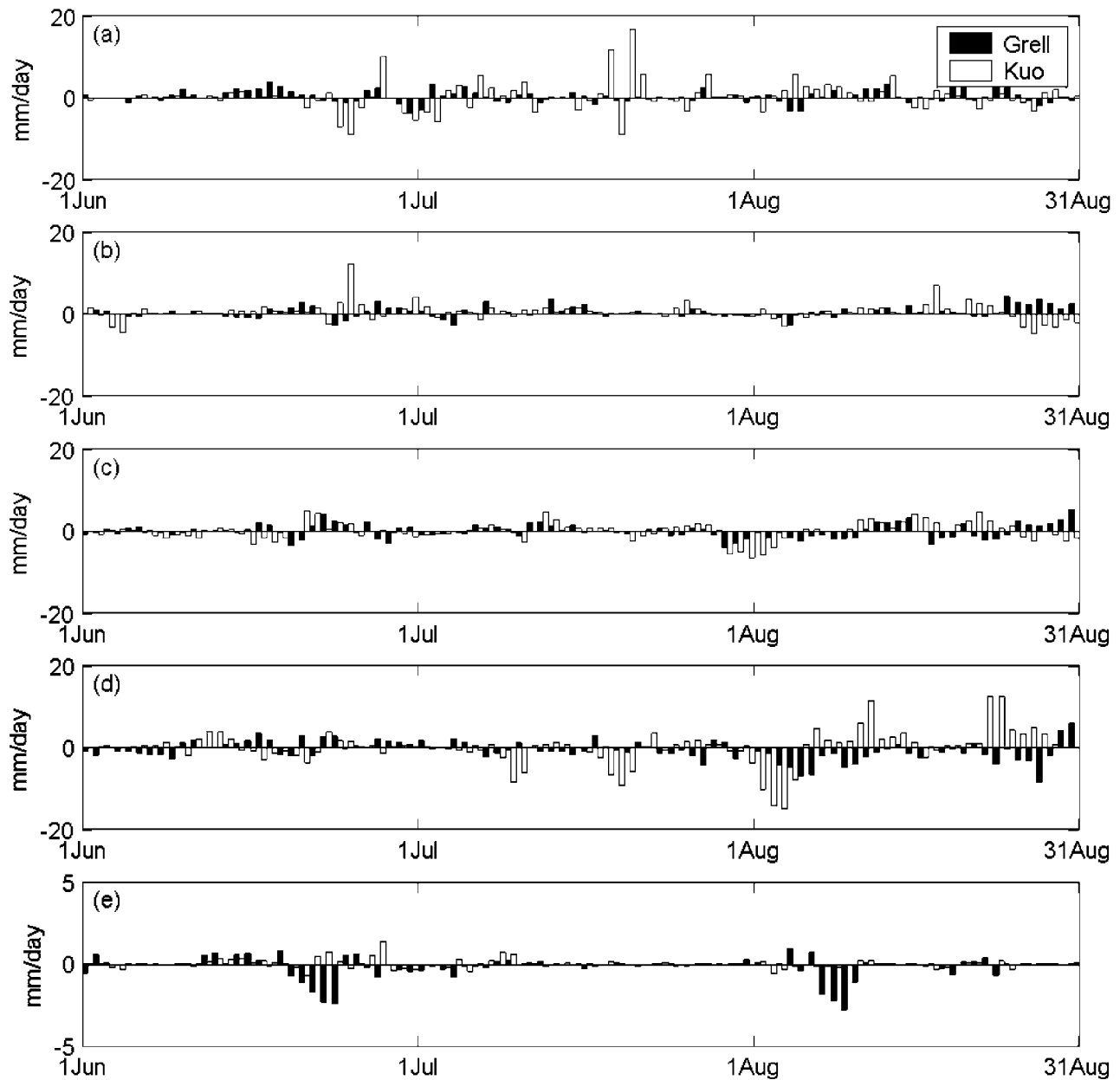
Figure 9. Daily time series of differences (RegCM3_GW minus RegCM3) in convective precipitation based on Grell scheme and Kuo scheme averaged over the subdomains. Regions (a) MSH1, (b) DSA2, (c) MHU3, (d) SHU4, and (e) DAR5.

heat and moisture characteristics of the boundary layer, and alter the convective instability. The changes of the boundary layer structure will affect the development of precipitation, and ultimately have impact on the soil moisture and groundwater through infiltration. This process is called the local feedback between the aquifer and atmosphere. On the other hand, large-scale variations of water table affect the horizontal distribution of soil moisture, which influences the spatial heterogeneity of land surface conditions and the large-scale circulation. The changes of circulation are responsible for the variations of atmospheric water vapor transport and the precipitable water, and finally influence

the precipitation. Such process accounts for the groundwater-atmosphere interaction in a regional scale.

5. Conclusion

[29] In this study, we develop a coupled regional climate model RegCM3_GW with a groundwater component and investigate the effects of water table dynamics on regional climate with the model. The simulations with RegCM3_GW and RegCM3 suggest that dynamical representation of water table in a regional climate model changes the surface heat and moisture fluxes through modifying the vertical profile of soil moisture, and the differences of simulated
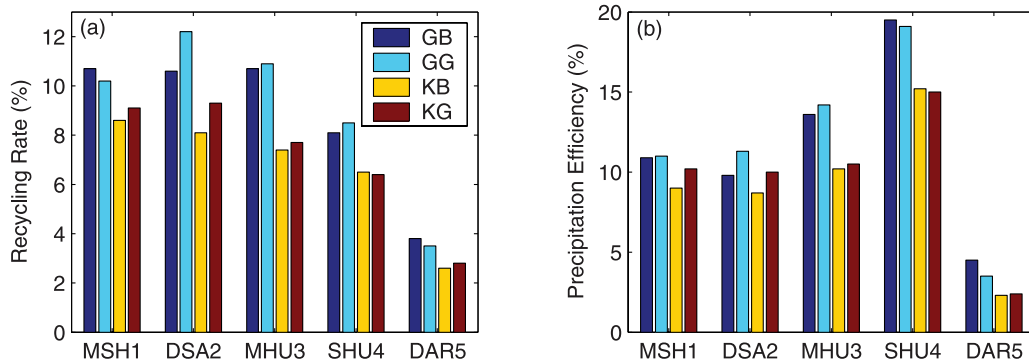
Figure 10. Comparisons of water cycle indices resulted from different models and different convective schemes over the five regions. GB, GG, KB, and KG are for RegCM3 with Grell scheme, RegCM3_GW with Grell scheme, RegCM3 with Kuo scheme, and RegCM3_GW with Kuo scheme, respectively.

surface fluxes result in different structures of the boundary layer and ultimately affect the convection. The cooling effect of the increased evapotranspiration (ET) on low-level atmosphere and the heating effect of the latent heat released by condensation on upper atmosphere contribute to the changes of wind field via thermal wind relation, and the local water table-induced variations of water vapor can affect the nearby places through the advection, which indicates that the feedback between groundwater and atmosphere cannot be explained by local land-atmosphere interaction alone, and hence, the macroscale atmospheric processes should be analyzed.

[30] Furthermore, we analyze the local water cycle including water table, soil moisture, ET and convective precipitation (P_{con}), and the atmospheric moisture budget in the selected subdomains, from simulations with two cumulus convection schemes. It is demonstrated that the topsoil layers become wetter and enhance the bare soil evaporation, the root zone soil layers also become wetter over monsoon area, but their relations with transpirations are not obvious. Atmospheric water budget analysis shows that water table dynamics increase recycling rate and precipitation efficiency greatly over semiarid regions, which is benefited from the positive feedback among the groundwater, soil moisture, ET and P_{con}. The variances of the series for P_{con} differences simulated by Grell convection scheme are smaller than that by Kuo convection scheme, which indicates that the effects of water table dynamics on the simulated P_{con} are stronger for the Kuo scheme than that for the Grell scheme. Nevertheless, both of the convection
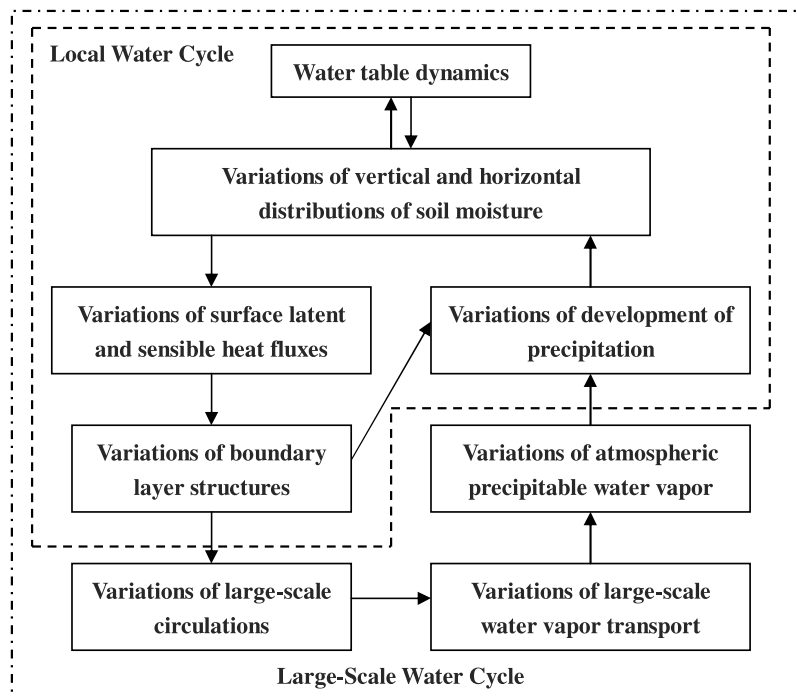
Figure 11. Schematic chart of the mechanism for the aquifer-atmosphere interaction.

schemes indicate that the groundwater-atmosphere feedbacks during summer over the east Asian monsoon area are presented in a regional scale, not limited in a separate subdomain.

References

Alley, W. M., R. W. Healy, J. W. LaBaugh, and T. E. Reilly (2002), Flow and storage in groundwater systems, *Science*, *296*, 1985–1990, doi:10.1126/science.1067123.

Anthes, R. A., E. Y. Hsie, and Y. H. Kuo (1987), Description of the Penn State/NCAR Mesoscale Model Version 4 (MM4), *NCAR Tech. Note, NCAR/TN-282+STR*, 66 pp., Natl. Cent. for Atmos. Res., Boulder, Colo.

Anyah, R. O., C. P. Weaver, G. Miguez-Macho, Y. Fan, and A. Robock (2008), Incorporating water table dynamics in climate modeling: 3. Simulated groundwater influence on coupled land-atmosphere variability, *J. Geophys. Res.*, *113*, D07103, doi:10.1029/2007JD009087.

Chen, X., and Q. Hu (2004), Groundwater influences on soil moisture and surface evaporation, *J. Hydrol. Amsterdam*, *297*, 285–300, doi:10.1016/j.jhydrol.2004.04.019.

Cosgrove, B. A., et al. (2003), Land surface model spin-up behavior in the North American Land Data Assimilation System (NLDAS), *J. Geophys. Res.*, *108*(D22), 8845, doi:10.1029/2002JD003316.

Dai, A., F. Giorgi, and K. E. Trenberth (1999), Observed and model-simulated diurnal cycles of precipitation over the contiguous United States, *J. Geophys. Res.*, *104*(D6), 6377–6402, doi:10.1029/98JD02720.

Dickinson, R. E. (1984), Modeling evapotranspiration for three-dimensional global climate models, in *Climate Processes and Climate Sensitivity, Geophys. Monogr. Ser.*, vol. 29, edited by J. E. Hansen and T. Takahashi, pp. 58–72, AGU, Washington, D. C.

Dickinson, R. E., A. Henderson-Seller, and P. J. Kennedy (1993), Biosphere-Atmosphere Transfer Scheme (BATS) version 1e as coupled to the NCAR Community Climate Model, *NCAR Tech. Rep. TN-387+STR*, 72 pp., Natl. Cent. for Atmos. Res., Boulder, Colo.

Emanuel, K. A., and M. Zivkovic-Rothman (1999), Development and evaluation of a convection scheme for use in climate models, *J. Atmos. Sci.*, *56*, 1766–1782, doi:10.1175/1520-0469(1999)056<1766:DAEOAC>2.0.CO;2.

Fan, Y., G. Miguez-Macho, C. P. Weaver, R. Walko, and A. Robock (2007), Incorporating water table dynamics in climate modeling: 1. Water table observations and equilibrium water table simulations, *J. Geophys. Res.*, *112*, D10125, doi:10.1029/2006JD008111.

Fritsch, J. M., and C. F. Chappell (1980), Numerical prediction of convectively driven mesoscale pressure systems. Part I: Convective parameterization, *J. Atmos. Sci.*, *37*, 1722–1733, doi:10.1175/1520-0469(1980)037<1722:NPOCDM>2.0.CO;2.

Georgescu, M., C. P. Weaver, R. Avissar, R. L. Walko, and G. Miguez-Macho (2003), Sensitivity of model-simulated summertime precipitation over the Mississippi River Basin to the spatial distribution of initial soil moisture, *J. Geophys. Res.*, *108*(D22), 8855, doi:10.1029/2002JD003107.

Giorgi, F. (1991), Sensitivity of simulated summertime precipitation over the western United States to physics parameterizations, *Mon. Weather Rev.*, *119*, 2870–2888, doi:10.1175/1520-0493(1991)119<2870:SOSSPO>2.0.CO;2.

Giorgi, F., R. Franciscco, and J. S. Pal (2003), Effects of subgrid-scale topography and land use scheme on the simulation of surface climate and hydrology. Part I: Effects of temperature and water vapor disaggregation, *J. Hydrometeorol.*, *4*, 317–333, doi:10.1175/1525-7541(2003)4<317:EOASTA>2.0.CO;2.

Grell, G. A. (1993), Prognostic evaluation of assumptions used by cumulus parameterizations, *Mon. Weather Rev.*, *121*, 764–787, doi:10.1175/1520-0493(1993)121<0764:PEOAUB>2.0.CO;2.

Grell, G. A., J. Dudhia, and D. R. Stauffer (1994), Description of the fifth generation Penn State/NCAR Mesoscale Model (MM5), *NCAR Tech. Rep. TN-398+STR*, 121 pp., Natl. Cent. for Atmos. Res., Boulder, Colo.

Gutowski, W. J., Jr, C. J. Vörösmarty, M. Person, Z. Ötles, B. Fekete, and J. York (2002), A Coupled Land-Atmosphere Simulation Program (CLASP): Calibration and validation, *J. Geophys. Res.*, *107*(D16), 4283, doi:10.1029/2001JD000392.

Holtslag, A. A. M., and B. A. Boville (1993), Local versus nonlocal boundary-layer diffusion in a global climate model, *J. Clim.*, *6*, 1825–1842, doi:10.1175/1520-0442(1993)006<1825:LVNBLD>2.0.CO;2.

Hostetler, S. W., G. T. Bates, and F. Giorgi (1993), Interactive nesting of a lake thermal model within a regional climate model for climate change studies, *J. Geophys. Res.*, *98*(D3), 5045–5058, doi:10.1029/92JD02843.

Kiehl, J. T., et al. (1996), Description of the NCAR Community Climate Model (CCM3), *NCAR Tech. Rep. NCAR/TN-420+STR*, 152 pp., Natl. Cent. for Atmos. Res., Boulder, Colo.

Koster, R. D., and M. J. Suarez (2001), Soil moisture memory in climate models, *J. Hydrometeorol.*, *2*, 558–570, doi:10.1175/1525-7541(2001)002<0558:SMMICM>2.0.CO;2.

Koster, R. D., M. J. Suarez, and M. Heiser (2000), Variance and predictability of precipitation at seasonal-to-interannual timescales, *J. Hydrometeorol.*, *1*, 26–46, doi:10.1175/1525-7541(2000)001<0026:VAPOPA>2.0.CO;2.

Koster, R. D., M. J. Suarez, R. W. Higgins, and H. M. Van de Dool (2003), Observational evidence that soil moisture variations affect precipitation, *Geophys. Res. Lett.*, *30*(5), 1241, doi:10.1029/2002GL016571.

Liang, X., and Z.-H. Xie (2003), Important factors in land-atmosphere interactions: Surface runoff generations and interactions between surface and groundwater, *Global Planet. Change*, *38*, 101–114, doi:10.1016/S0921-8181(03)00012-2.

Liang, X., Z.-H. Xie, and M. Huang (2003), A new parameterization for surface and groundwater interaction and its impact on water budgets with the variable infiltration capacity (VIC) land surface model, *J. Geophys. Res.*, *108*(D16), 8613, doi:10.1029/2002JD003090.

Liang, X.-Z., M. Xu, K. E. Kunkel, G. A. Grell, and J. S. Kain (2007), Regional climate model simulation of U.S.-Mexico summer precipitation using the optimal ensemble of two cumulus parameterizations, *J. Clim.*, *20*, 5201–5207, doi:10.1175/JCLI4306.1.

Maxwell, R. M., and N. L. Miller (2005), Development of a coupled land surface and groundwater model, *J. Hydrometeorol.*, *6*, 233–247, doi:10.1175/JHM422.1.

Miguez-Macho, G., Y. Fan, C. P. Weaver, R. Walko, and A. Robock (2007), Incorporating water table dynamics in climate modeling: 2. Formulation, validation, and soil moisture simulation, *J. Geophys. Res.*, *112*, D13108, doi:10.1029/2006JD008112.

Niu, G.-Y., Z.-L. Yang, R. E. Dickinson, L. E. Gulden, and H. Su (2007), Development of a simple groundwater model for use in climate models and evaluation with Gravity Recovery and Climate Experiment data, *J. Geophys. Res.*, *112*, D07103, doi:10.1029/2006JD007522.

Pal, J. S., E. E. Small, and E. A. B. Eltahir (2000), Simulation of regional scale water and energy budgets: Influence of a new moist physics scheme within RegCM, *J. Geophys. Res.*, *105*, 29,579–29,594, doi:10.1029/2000JD900415.

Pal, J. S., et al. (2007), Regional climate modeling for the developing world: The ICTP RegCM3 and RegCNET, *Bull. Am. Meteorol. Soc.*, *88*, 1395–1409, doi:10.1175/BAMS-88-9-1395.

Pan, Z.-T., E. Takle, M. Segal, and R. Turner (1996), Influences of model parameterization schemes on the response of rainfall to soil moisture in the central United States, *Mon. Weather Rev.*, *124*, 1786–1802, doi:10.1175/1520-0493(1996)124<1786:IOMPSO>2.0.CO;2.

Qian, T., A. Dai, K. E. Trenberth, and K. W. Oleson (2006), Simulation of global land surface conditions from 1948–2004. Part I: Forcing data and evaluation, *J. Hydrometeorol.*, *7*, 953–975, doi:10.1175/JHM540.1.

Schär, C., D. Lüthi, U. Beyerle, and E. Heise (1999), The soil-precipitation feedback: A process study with a regional climate model, *J. Clim.*, *12*, 722–741, doi:10.1175/1520-0442(1999)012<0722:TSPFAP>2.0.CO;2.

Xie, P.-P., M. Chen, S. Yang, A. Yatagai, T. Hayasaka, Y. Fukushima, and C. Liu (2007), A gauge-based analysis of daily precipitation over east Asia, *J. Hydrometeorol.*, *8*, 607–626, doi:10.1175/JHM583.1.

Xie, Z.-H., Q.-C. Zeng, Y.-J. Dai, and B. Wang (1998), Numerical simulation of an unsaturated flow equation, *Sci. China*, *41*(D), 429–436.

Xie, Z.-H., Q.-C. Zeng, and Y.-J. Dai (1999), An unsaturated soil flow problem and its numerical simulation, *Adv. Atmos. Sci.*, *16*(2), 183–196.

Yang, H.-W., and Z.-H. Xie (2003), A new method to dynamically simulate groundwater table in land surface model VIC, *Prog. Nat. Sci.*, *13*(11), 819–825, doi:10.1080/10020070312331344490.

Yang, Z.-L., R. E. Dickinson, A. Henderson-Sellers, and A. J. Pitman (1995), Preliminary study of spin-up processes in land surface models with the first stage data of Project for Intercomparison of Land Surface Parameterization Schemes Phase 1 (a), *J. Geophys. Res.*, *100*(D8), 16,553–16,578, doi:10.1029/95JD01076.

Yeh, P. J.-F., and E. A. B. Eltahir (2005a), Representation of water table dynamics in a land surface scheme, part I: Model development, *J. Clim.*, *18*, 1861–1880, doi:10.1175/JCLI3330.1.

Yeh, P. J.-F., and E. A. B. Eltahir (2005b), Representation of water table dynamics in a land surface scheme, part II: Subgrid variability, *J. Clim.*, *18*, 1881–1901, doi:10.1175/JCLI3331.1.

York, J. P., M. Person, W. J. Gutowski, and T. C. Winter (2002), Putting aquifers into atmospheric simulation models: An example from the Mill Creek watershed, northeastern Kansas, *Adv. Water Resour.*, *25*(2), 221–238, doi:10.1016/S0309-1708(01)00021-5.

Yuan, X., Z.-H. Xie, and M.-L. Liang (2008), Spatiotemporal prediction of shallow water table depths in continental China, *Water Resour. Res.*, *44*, W04414, doi:10.1029/2006WR005453.

Zeng, X., M. Zhao, and R. E. Dickinson (1998), Intercomparison of bulk aerodynamic algorithms for the computation of sea surface fluxes using TOGA COARE and TAO data, *J. Clim.*, *11*, 2628–2644, doi:10.1175/1520-0442(1998)011<2628:IOBAAF>2.0.CO;2.

_____

X. Tian, Z. Xie, X. Yuan, and J. Zheng, Institute of Atmospheric Physics, Chinese Academy of Sciences, Beijing 100029, China. (zxie@lasg.iap.ac.cn)

Z. Yang, Department of Geological Sciences, University of Texas, Austin, TX 78712, USA.